Spin orbit torque induced asymmetric depinning of chiral Néel domain wall in Co/Ni heterostructures

Journal Item

Spin orbit torque induced asymmetric depinning of chiral Néel domain wall in Co/Ni heterostructures

M. Ramu, S. Goolaup, W. L. Gan, S. Krishnia, G. J. Lim, and W. S. Lew

Citation: Appl. Phys. Lett. **110**, 162402 (2017); doi: 10.1063/1.4980120
View online: http://dx.doi.org/10.1063/1.4980120
View Table of Contents: http://aip.scitation.org/toc/apl/110/16
Published by the American Institute of Physics

Spin orbit torque induced asymmetric depinning of chiral Néel domain wall in Co/Ni heterostructures

M. Ramu, S. Goolaup, W. L. Gan, S. Krishnia, G. J. Lim, and W. S. Lew[a)]
School of Physical and Mathematical Sciences, Nanyang Technological University, 21 Nanyang Link, Singapore 637371

(Received 19 January 2017; accepted 2 April 2017; published online 20 April 2017)

In this letter, we report on distinct depinning of a chiral Néel domain wall (DW) driven by spin-orbit torque (SOT) in Co/Ni nanowires with symmetric potential barriers. In these structures, DW propagation was shown to be in the opposite direction to the electron flow as evidenced from current assisted DW depinning measurements. A transition from field dominated DW depinning to SOT dominated DW depinning was observed as the bias current was increased. For SOT dominated DW depinning, the Up-Down DW exhibits a larger depinning field as compared to the Down-Up DW. This is attributed to the interplay between the SOT and Dzyaloshinskii-Moriya interaction in the structure. *Published by AIP Publishing.* [http://dx.doi.org/10.1063/1.4980120]

Domain wall (DW) dynamics in ferromagnetic nanowires (NWs) have been extensively investigated for the realization of scalable low power non-volatile memory and spin logic devices.[1–3] In bulk ferromagnets, adiabatic spin transfer torque (STT) is responsible for current induced domain wall motion (CIDM).[4,5] The onset of STT driven DW motion is via the transformation of the internal spin structure from Bloch to Néel.[6,7] However, in ultrathin magnetic heterostructures, a Néel DW can be stabilized by a Dzyaloshinskii-Moriya interaction (DMI), which is an antisymmetric exchange interaction in a ferromagnetic system arising from the broken inversion symmetry and strong spin orbit coupling (SOC).[8–10] It induces an effective field (H_{DMI}) that promotes a chiral Néel DW.[11] Additionally, the strong SOC in these materials can generate current induced spin-orbit torques (SOTs) through the spin Hall effect (SHE) and the Rashba effect (RE).[12–16] These effects produce Slonczewski-like and field-like torques. The Slonczewski-like torque is phenomenologically equivalent to the conventional spin transfer torque, and it contributes to the efficient driving of Néel DWs. On the other hand, the effective field from field-like torque, which lies in-plane and transverse to the current direction, does not contribute to the DW dynamics, but it can alter the DW internal magnetization.[17] The detection of the DW in perpendicularly magnetized NWs has been performed via Hall cross structures.[18] Such structures introduce potential landscapes for the DW propagation. There have been several experimental reports on pinning and depinning of the DW driven by bulk STT.[19] But SOT driven DW depinning in ultrathin NWs is still elusive.

Here, we explore chiral Néel DW depinning driven by SOT in perpendicularly magnetized Co/Ni heterostructures. The DC bias current dependence reveals that field induced DW depinning is dominant for smaller DC currents, while SOT is responsible for DMI induced chiral Néel DW depinning at larger currents. Additionally, for larger currents, different depinning efficiencies for Up-Down and Down Up DWs were observed. The difference in the depinning fields between Up-Down and Down-Up DWs was found to be increased. The SOT in concert with DMI was attributed to this behaviour.

NWs with symmetrical Hall crosses were patterned by electron beam lithography and ion milling techniques from a thin film stack of Ta (5)/Pt (5)/[Co (0.25)/Ni (0.5)]$_4$/Co (0.25)/Ru (5). To break the structural inversion symmetry, two different heavy metals, Pt and Ru, were chosen as seed and capping layers, respectively. The thin film stack was deposited on a thermally oxidized Si wafer (300 nm thick SiO_2) by DC magnetron sputtering. A scanning electron microscopy (SEM) image of the NW together with a schematic of the measurement setup is shown in Fig. 1(a). Two Ta (5)/Cu (80)/Au (20) electrodes labelled A and B were patterned on top of the NW to nucleate and drive the DW, respectively. Alternating gradient field magnetometer measurements reveal that the film has a perpendicular magnetic anisotropy (PMA) with an effective anisotropy constant K_{eff} of 1.24×10^6 erg/cc and a saturation magnetization M_s of 362 emu/cc. A DC bias current (I_{DC}) was injected via bias tee, which separates the DC current source from a pulse generator. The DW displacement was detected at the Hall cross through the anomalous Hall effect (AHE), which is proportional to the component of magnetization perpendicular to the NW. For DW nucleation, a pulse current of 80 mA with a duration of 50 ns was injected through electrode A. The normalized Hall resistance (R_{Hall}) for a 300 nm wide NW, without any DW injected, while an external magnetic field is swept along the z-axis, is shown in Fig. 1(b). The normalized R_{Hall} value of 1 (0) corresponds to upward ($+z$) (downward ($-z$)) orientation of magnetization in the Hall cross. A clear square hysteresis loop with a coercive field of ~900 Oe confirms that the magnetic easy axis of the NW is perpendicular to the plane of the NW.

For DW dynamics measurement, a perpendicular magnetic field (H_z) of ~+2 kOe was initially applied globally to obtain a single magnetization state along the $+z$ (Up) orientation in the NW. A current pulse is then injected through the electrode A to nucleate a ↓↑ DW on the right edge of the

[a)]Author to whom correspondence should be addressed. Electronic mail: wensiang@ntu.edu.sg

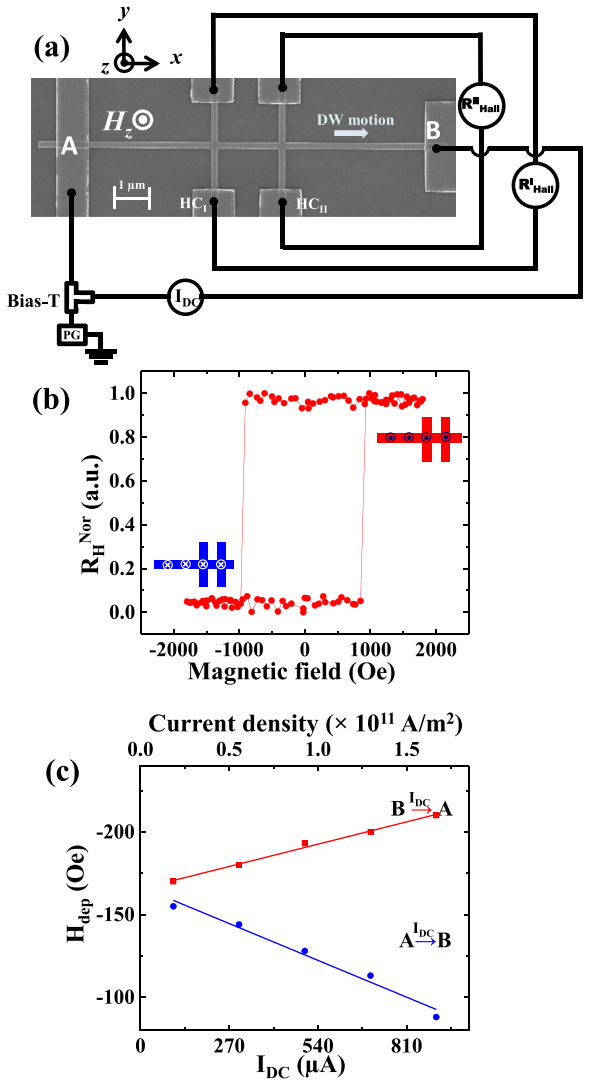

FIG. 1. (a) Scanning electron microscopy image of the device with a schematic measurement setup. The device comprises of a Co/Ni NW with two Hall crosses labelled as HC_I and HC_{II} and two Ta/Cu/Au electrodes (A and B). (b) Normalized Hall resistance (R_{Hall}), without any DW injected, as a function of sweeping external magnetic field along the out-of-plane direction. (c) Linear dependence of the DW depinning field (H_{dep}) as a function of DC bias current (I_{DC}) applied along A → B (blue plot) and B → A (red plot).

electrode A. Similarly, the ↑↓ DW can also be injected by setting the initial magnetization of the NW along the $-z$ (down) orientation. The application of an external out-of-plane field drives the DW towards electrode B, the opposite edge of the NW. The critical field (H_{dep}) required for the DW to overcome the potential barrier at the Hall crosses can be inferred from the AHE measurement. To understand the effect of DC bias current on the DW depinning process, DC currents with varying amplitudes were applied from A → B and B → A. For currents applied from A → B (B → A), the direction of the current is parallel (anti parallel) to the DW motion. Note that the direction of the DW motion, from electrodes A to B, is governed solely by the external out-of-plane field, while I_{DC} assists or opposes the DW motion. The maximum value of I_{DC} was limited to 900 μA so as to negate any thermal effects that may influence the DW motion. The corresponding depinning fields, H_{dep}, measured for each DC bias current is plotted in Fig. 1(c). The current density has been computed by considering the current passing through the whole stack and is shown as the x_2 axis in Fig. 1(c). H_{dep} varies linearly as a function of I_{DC} for both directions of the current flow, but it exhibits opposite slopes as a function of the magnitude of the current. When I_{DC} is applied from B → A, while the DW moves from A → B, the magnitude of H_{dep} increases with I_{DC}. However, an opposite trend was obtained for I_{DC} applied from A → B. The observed results suggest that the DW motion is being assisted along the current flow direction. The strength of the potential barrier at the Hall cross was obtained by extrapolating H_{dep} to $I_{DC} = 0$ and was estimated to be ∼165 Oe. The slope of H_{dep} *vs* j_e gives the depinning efficiency ($|\Delta H_{dep}|/|\Delta J|$) and is computed to be ∼15 and ∼25 Oe per 10^{11} Am^{-2} for currents applied from B → A and A → B, respectively. The difference in the depinning efficiencies for the two current directions suggests that the depinning efficiency is highly dependent on the direction of current. These results cannot be explained with the prediction of the conventional bulk spin transfer torque effect, where one would expect the lowering of the H_{dep} for the DW moving in the direction of the electron flow (i.e., current flows from B → A). Instead, an alternative mechanism whereby a DMI induced chiral Néel DW driven by spin orbit torques may account for these observed results. Joule heating does not influence the DW depinning process in our experiment. For the whole range of DC bias currents investigated, the temperature of the NW was monitored by measuring the resistance of the NW. The wire resistance did not exhibit any appreciable change, implying that the joule heating effect is negligibly small in our sample. Additionally, if the joule heating effect were present, irrespective of the direction of I_{DC}, a lower depinning field and a deviation from the linear behaviour of the current dependent H_{dep} would have been observed.

To confirm that chiral DW structures are stabilized in our NW, the DMI in our sample stack was evaluated. The strength of DMI in our stack structure was measured using the field induced DW creep method.[11] The DW expansion was observed by a wide field Kerr microscope equipped with two electromagnets that generate both in-plane and out-of-plane magnetic fields. The representative Kerr images are shown as insets in Fig. 2(a). As shown in the top middle inset, where the in-plane field $H_x = 0$, the domain expansion is expected to be symmetric with respect to an axis parallel to the out-of-plane field. The symmetry is broken when an in-plane field is applied in conjunction with the out-of-plane field. The domain expansion driven by a fixed out-of-plane field of 10 mT Oe under an in-plane bias field of ∼80 mT pointing in $-x$ and $+x$ directions is shown in bottom left and bottom right insets, respectively. For instance, when an in-plane field is applied along the $-x$ direction, right and left DWs move with different velocities. It results in the asymmetric expansion of the domain. The asymmetric expansion of the domain confirms that the magnetization inside the DW rotates anti-clockwise with left handed chirality, and hence, DMI is negative. As shown in Fig. 2(a), the two velocity plots shift away from $H_x = 0$ in opposite directions. The field at which the minimum velocity occurs, ∼45 mT in our sample, provides an estimate of the DMI field, $H_{DMI} = -45$ mT. The

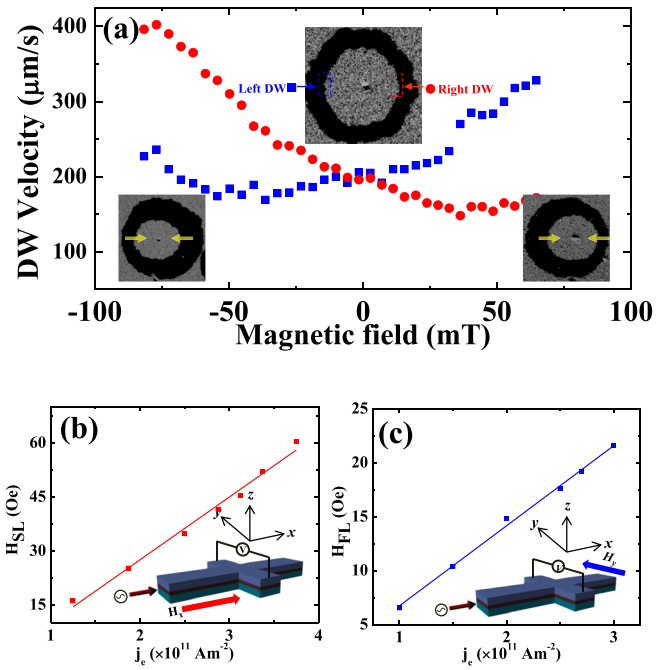

FIG. 2. (a) DW velocity as a function of in-plane bias field for left (blue plot) and right (red dots) DWs. The inset in the top middle represents a differential Kerr image of isotropic domain expansion driven by the out-of-plane field (H_Z), where in-plane field $H_x = 0$. The Kerr image for anisotropic domain expansion when an in-plane field is applied along the directions $-H_x$ (bottom right inset) and $+H_x$ (bottom left inset). Dark contrast represents a Up domain, while arrows indicate the equilibrium magnetization direction within the DW. Current induced effective fields (H_{SL}) and (H_{FL}) as a function of current density (j_e) applied longitudinal (b) and transverse (c) to the NW. Solid lines are the fitted curves, and the inset shows the schematic measurement setup.

DMI constant was estimated (the calculation is shown in the supplementary material).

For our thin film stack, the magnetic multilayer [Co/Ni]$_4$/Co is sandwiched between two heavy metals Pt (5 nm) and Ru (5 nm). The spin Hall angle (θ_{SHE}) of Ru is negligibly small and has a positive sign.[20] As such, the significant source of spin current is expected to be from the Pt layer. Since Pt has a positive spin Hall angle $\theta_{SHE} > 0$, the left-handed Néel DW is expected to move along the current flow direction. This is consistent with our observed experimental results from the DMI measurement. To quantify the strength of the SOT induced effective fields in our sample, an AC harmonic measurement scheme was employed.[21] The schematics of the measurement set-up for characterizing the Slonczewski like (H_{SL}) and field like (H_{FL}) effective fields are shown in the inset of Figs. 2(b) and 2(c), respectively. An AC current with a frequency of 330 Hz was passed through the NW, and an in-plane field was simultaneously swept along or transverse to the NW long axis. The AC induced effective fields are given by the following equation:[21]

$$H_{SL(FL)} = -2\frac{\dfrac{\partial V_{2\omega}}{\partial H_{SL(FL)}}}{\dfrac{\partial^2 V_{\omega}}{\partial H^2{}_{SL(FL)}}}, \tag{1}$$

where V_ω and $V_{2\omega}$ are the first and second harmonics of the Hall voltage, measured by a lock-in amplifier. The SOT induced effective fields extracted using Eq. (1) vary linearly with J_e, as shown in Figs. 2(b) and 2(c). The Slonczewski-like effective field, H_{SL}, was computed to be ~15 Oe per 10^{11} A/m^2, and the field-like field, H_{FL}, was 7 Oe per 10^{11} A/m^2.

To further investigate the effect of DMI and SOT on the DW dynamics for both ↑↓ and ↓↑ DWs, the depinning experiments were repeated in a 500 nm wide NW. In order to move both ↑↓ and ↓↑ DWs in the same direction for the detection at the Hall cross, the sign of the H_z field was reversed, and the current was passed along the direction of the field induced DW propagation. Fig. 3(a) shows H_{dep} as a function of I_{DC} applied along A → B and B → A for both ↑↓ and ↓↑ DWs. The corresponding current density is shown on the x_2 scale. As expected, for currents flowing along the DW propagation direction (A → B), the depinning field reduces linearly as the magnitude of the current is increased for both ↑↓ and ↓↑ DWs. Conversely, for DW motion opposing the current flow, the depinning field increases monotonically as a function of the magnitude of the current. As Pt has a positive spin hall angle, SOT induced DW motion will be along the direction of the applied current. For $I_{DC} \leq 300\,\mu$A, the magnitude of the depinning fields for different directions of the current and different types of DWs are almost the same.

However, for $I_{DC} > 300\,\mu$A, both ↑↓ and ↓↑ DWs exhibit different depinning fields with respect to different bias currents. Fig. 3(b) shows the magnitude of the depinning field for symmetrical ↑↓ and ↓↑ DWs as a function of the current applied from A → B. In both instances, the current assists the DW propagation. Interestingly, distinct depinning fields are observed for ↑↓ and ↓↑ DWs. As the current is increased, the difference in the depinning fields also increases. In our sample stack, the left handed Nèel DW is the stable DW configuration as demonstrated by the DMI measurement. Fig. 3(c) illustrates the directions of the current induced effective fields (H_{SL} and H_{FL}) acting on the left handed Nèel DW of both ↑↓ and ↓↑. For a ↑↓ DW with its internal magnetization stabilized along the $-x$ direction, the effective field due to the Slonczewski-like torque should be aligned along $(m \times (z \times j_e))$ or the z direction, where m, z, and j_e represent unit vectors along magnetization, z-axis and electron flow, respectively. Similarly, for a ↓↑ DW, H_{SL} should be oriented along the $+z$ direction. For these two DWs, the applied out-of-plane field (H_z) and Slonczewski-like effective field (H_{SL}) act in concert, which results in the same depinning field. The observed asymmetry in the depinning fields for ↑↓ and ↓↑ DWs thus cannot be ascribed to the H_{SL}. Different devices have been tested and confirmed that this depinning anomaly is not due to structural irregularities or the edge defects. Our AC harmonic measurements reveal that the magnitude of the current induced effective field, $H_{FL} = \sim 7$ Oe per 10^{11} Am^{-2}, due to field-like torque is comparable to the $H_{SL} = \sim 14$ Oe per 10^{11} Am^{-2}. The H_{FL} can be described simply by an external magnetic field that lies in-plane and transverse to the current direction, and the magnitude of H_{FL} scales linearly with current. Unlike H_{SL}, H_{FL} does not contribute to the DW motion, but it alters the DW internal magnetization. As shown in Fig. 3(c), the direction of H_{FL} is fixed along $(z \times j_e)$ or the $-y$-axis for both ↑↓ and ↓↑ DWs. The resultant Zeeman interaction tilts the DW moment in the same direction as the DW propagation for ↓↑ DW, while it tilts the DW moment in the direction opposite to the current direction

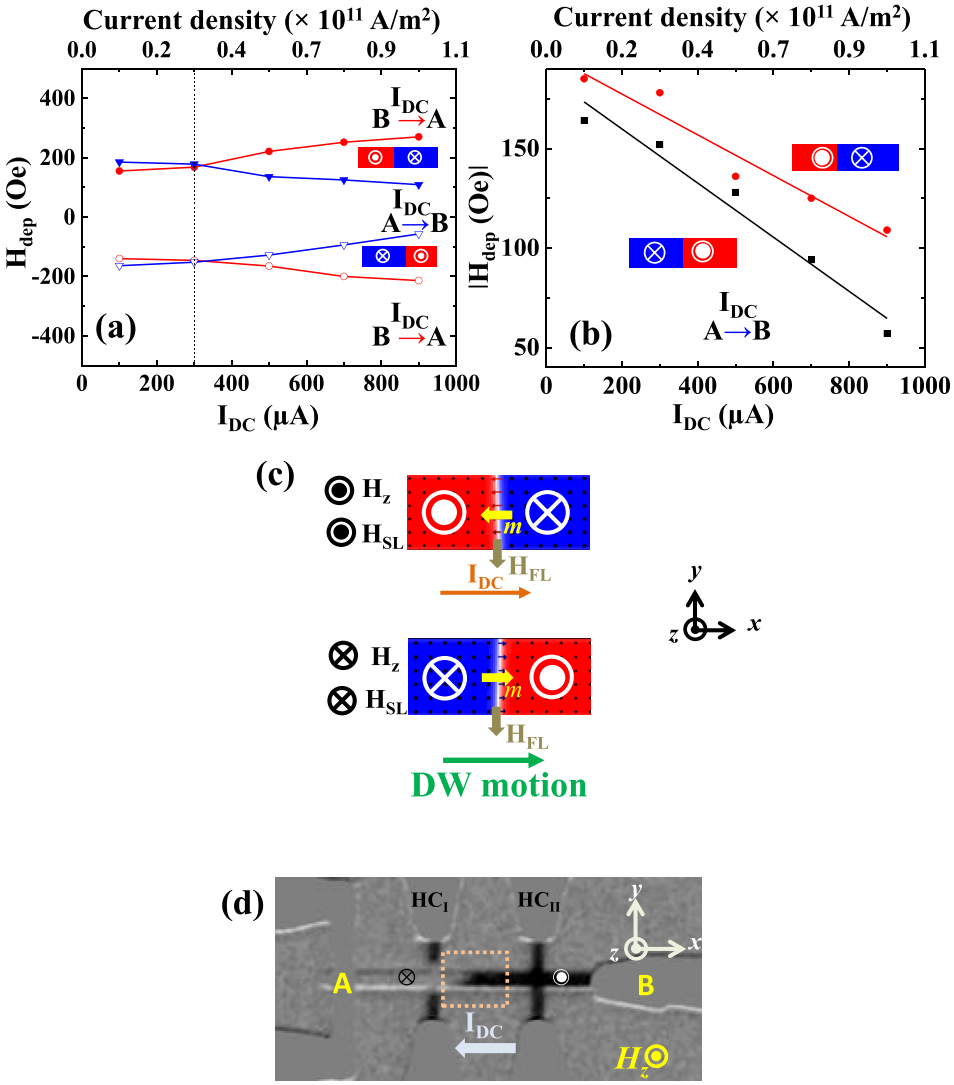

FIG. 3. (a) H_{dep} as a function of I_{DC} applied along A → B and B → A for ↑↓ and ↓↑ DWs. (b) Magnitude of the H_{dep} as a function of I_{DC} applied along A → B for both DWs. (c) Schematic of directions of the current induced effective fields (H_{SL}, H_{FL}) acting on the left handed Nèel DW of both ↑↓ and ↓↑. H_z indicates the perpendicular field applied to drive the DW. I_{DC} is applied along the direction of field induced DW motion. (d) Kerr imaging of a tilted DW as it propagates through the NW. I_{DC} is applied in a direction opposite to the DW motion. The dotted area shows the DW magnetization orientation.

for ↑↓ DW. The strength of H_{FL} increases with higher applied current, which in turn enlarges the degree of DW tilt in the respective directions for ↑↓ and ↓↑ DWs. Consequently, ↓↑ DW has a low depinning field compared to that of ↑↓ DW.

Ex-situ polar Kerr microscopy was used to obtain the DW configuration after it depins from the Hall cross I. For this measurement, we chose a 1 μm wide NW for ease of imaging and the Hall crosses are separated by a distance of 10 μm. A DW was nucleated in the NW, and the simultaneous application of a perpendicular magnetic field sweeping along the negative ($-z$) direction together with I_{DC} was used to drive the DW. Fig. 3(d) shows the Kerr image of the DW after it depins from the Hall cross I. The DW tilting can be clearly seen (dotted square) as it propagates along the NW under the application of the perpendicular field and current. It is also observed that the branches of the Hall cross I were not completely switched. This confirms that the current dominates the DW depinning process at the Hall cross.

In summary, we have investigated DMI induced chiral Néel DW depinning driven by SOT in perpendicularly magnetized Co/Ni NWs with symmetric Hall crosses. In these structures, DMI stabilizes left handed chiral Neel DW. A cross over from field induced DW depinning to SOT driven DW depinning was observed as the DC bias current was increased. For SOT assisted DW motion, the Down-Up DW exhibits a larger depinning field as compared to the Up/Down DW. This is attributed to the current induced SOT in concert with DMI.

See supplementary material for the estimation of DMI constant, the effect of the width variation on domain wall depinning, and micromagnetic simulations of domain wall depinning through Hall crosses.

This work was supported by the Singapore National Research Foundation, Prime Minister's Office, under a Competitive Research Programme (Non-volatile Magnetic Logic and Memory Integrated Circuit Devices, No. NRF-CRP9-2011-01), and an Industry-IHL Partnership Program (No. NRF2015-IIP001-001). The work was also supported by a MOE-AcRF Tier 2 Grant (No. MOE 2013-T2-2-017). The support from an RIE2020 AME-Programmatic Grant (No. A1687b0033) is also acknowledged. WSL is a member of the Singapore Spintronics Consortium (SG-SPIN).

[1]S. Parkin, M. Hayashi, and L. Thomas, Science **320**, 190 (2008).
[2]D. A. Allwood, G. Xiong, C. C. Faulkner, D. Atkinson, D. Petit, and R. P. Cowburn, Science **309**, 1688 (2005).
[3]S. Goolaup, M. Ramu, C. Murapaka, and W. S. Lew, Sci. Rep. **5**, 9603 (2015).

[4]L. Berger, J. Appl. Phys. **55**, 1954 (1984).
[5]J. Slonczweski, J. Magn. Magn. Mater. **159**, L1 (1996).
[6]L. Berger, J. Appl. Phys. **71**, 2721 (1992).
[7]G. Tatara and H. Kohno, Phys. Rev. Lett. **92**, 086601 (2004).
[8]T. Moriya, Phys. Rev. Lett. **4**, 228 (1960).
[9]M. Heide, G. Bihlmayer, and S. Blügel, Phys. Rev. B **78**, 140403 (2008).
[10]A. Thiaville, S. Rohart, E. Jue, V. Cros, and A. Fert, Europhys. Lett. **100**, 57002 (2012).
[11]S. G. Je, D. H. Kim, S. C. Yoo, B. C. Min, K. J. Lee, and S. B. Choe, Phys. Rev. B **88**, 214401 (2013).
[12]L. Liu, C. F. Pai, Y. Li, H. W. Tseng, D. C. Ralph, and R. A. Buhrman, Science **336**, 555 (2012).
[13]P. P. J. Haazen, E. Mure, J. H. Franken, R. Lavrijsen, H. J. M. Swagten, and B. Koopmans, Nat. Mater. **12**, 299 (2013).
[14]S. Emori, U. Bauer, S. M. Ahn, E. Martinez, and G. S. D. Beach, Nat. Mater. **12**, 611 (2013).
[15]I. M. Miron, G. Gaudin, S. Auffret, B. Rodmacq, A. Schuhl, S. Pizzini, J. Vogel, and P. Gambardella, Nat. Mater. **9**, 230 (2010).
[16]K. W. Kim, S. M. Seo, J. Ryu, K. J. Lee, and H. W. Lee, Phys. Rev. B **85**, 180404 (2012).
[17]A. V. Khvalkovskiy, V. Cros, D. Apalkov, V. Nikitin, M. Krounbi, K. A. Zvezdin, A. Anane, J. Grollier, and A. Fert, Phys. Rev. B **87**, 020402 (2013).
[18]T. Koyama, D. Chiba, K. Ueda, H. Tanigawa, S. Fukami, T. Suzuki, N. Ohshima, N. Ishiwata, N. Nakatani, and T. One, Appl. Phys. Lett. **98**, 192509 (2011).
[19]K. Y. Wang, A. C. Irvine, J. Wunderlich, K. W. Edmonds, A. W. Rushforth, R. P. Campion, C. T. Foxon, D. A. Williams, and B. L. Gallagher, New J. Phys. **10**, 085007 (2008).
[20]X. Qiu, W. Legrand, P. He, Y. Wu, J. Yu, R. Ramaswamy, A. Manchon, and H. Yang, Phys. Rev. Lett. **117**, 217206 (2016).
[21]J. Kim, J. Sinha, M. Hayashi, M. Yamanouchi, S. Fukami, T. Suzuki, S. Mitani, and H. Ohno, Nat. Mater. **12**, 240 (2013).